

Online Research @ Cardiff

This is an Open Access document downloaded from ORCA, Cardiff University's institutional repository: <https://orca.cardiff.ac.uk/id/eprint/122112/>

This is the author's version of a work that was submitted to / accepted for publication.

Citation for final published version:

Vorobyov, Vasily, Bakharev, Boris, Medvinskaya, Natalia, Nesterova, Inna, Samokhin, Alexander Deev, Tatarnikova, Olga, Ustyugov, Aleksey A, Sengpiel, Frank ORCID: <https://orcid.org/0000-0002-7060-1851> and Bobkova, Natalia 2019. Loss of midbrain dopamine neurons and altered apomorphine EEG effects in the 5xFAD mouse model of Alzheimer's disease. *Journal of Alzheimer's Disease* 70 (1) , pp. 241-256. 10.3233/JAD-181246 file

Publishers page: <https://doi.org/10.3233/JAD-181246>
<<https://doi.org/10.3233/JAD-181246>>

Please note:

Changes made as a result of publishing processes such as copy-editing, formatting and page numbers may not be reflected in this version. For the definitive version of this publication, please refer to the published source. You are advised to consult the publisher's version if you wish to cite this paper.

This version is being made available in accordance with publisher policies.

See

<http://orca.cf.ac.uk/policies.html> for usage policies. Copyright and moral rights for publications made available in ORCA are retained by the copyright holders.



Loss of midbrain dopamine neurons and altered apomorphine EEG effects in the 5xFAD mouse model of Alzheimer's disease

Vasily Vorobyov^a, Boris Bakharev^a, Natalia Medvinskaya^a, Inna Nesterova^a, Alexander Samokhin^a, Alexander Deev^b, Olga Tatarnikova^a, Aleksey A Ustyugov^c, Frank Sengpiel^d, Natalia Bobkova^a

^a*Institute of Cell Biophysics, Russian Academy of Sciences, 142290 Pushchino, Moscow Region, Russian Federation*

^b*Institute of Theoretical and Experimental Biophysics, Russian Academy of Sciences, 142290 Pushchino, Moscow Region, Russian Federation*

^c*Institute of Physiologically Active Compounds, Russian Academy of Sciences, 142432, Chernogolovka, Moscow Region, Russian Federation*

^d*School of Biosciences and Neuroscience & Mental Health Research Institute, Cardiff University, Museum Avenue, Cardiff CF10 3AX, UK*

Running head: *EEG in 5xFAD mice*

Corresponding author:

Dr. V. Vorobyov, PhD

Institute of Cell Biophysics

Pushchino, 142290

Russian Federation

Tel: 007-4967-739-223

Fax: 007-4967-330-509

E-mail: vorobyovv2@gmail.com

Abstract

Cognitive malfunction, synaptic dysfunction, and disconnections in neural networks are core deficits in Alzheimer's disease (AD). 5xFAD mice, a transgenic model of AD, are characterised by an enhanced level of amyloid-*beta* and abnormal neurotransmission. The dopaminergic (DA) system has been shown to be involved in amyloid-*beta* transformations and neuronal plasticity; however, its role in functional network changes in familial AD still remains unclear. In 5xFAD and non-transgenic freely moving mice, electroencephalograms (EEGs) were simultaneously recorded from the secondary motor cortex (MC), superficial layers of the hippocampal CA1 area (HPC), substantia nigra (SN), and ventral tegmental area (VTA). EEGs and their frequency spectra were analysed before and after systemic injection of a DA receptor agonist, apomorphine (APO). In the baseline EEG from MC and HPC of 5xFAD mice, *delta* and *alpha* oscillations were enhanced and *beta* activity was attenuated, compared to control mice. In VTA and SN of 5xFAD mice, *delta-theta* activity was decreased and *beta* oscillations dominated. In control mice, APO suppressed *delta* activity in VTA to a higher extent than in MC, whereas in 5xFAD mice, this difference was eliminated due to attenuation of the *delta* suppression in VTA. APO increased *beta* activity in MC of mice from both groups while significant *beta* suppression was observed in VTA of 5xFAD mice. These mice were characterized by significant decrease of tyrosine hydroxylase immunopositive cells in both VTA and SN and of DA transporter in MC and hippocampal dentate gyrus. We suggest that the EEG modifications observed in 5xFAD mice are associated with alterations in dopaminergic transmission, resulting in adaptive changes in the cerebral networks in the course of familial AD development.

Key words: secondary motor cortex; hippocampus; ventral tegmental area; substantia nigra; DAT; electroencephalogram; frequency spectrum

1. Introduction

Alzheimer's disease (AD), characterized by neurodegeneration, pathological formation of extracellular amyloid plaques and intraneuronal aggregation of hyperphosphorylated tau into neurofibrillary tangles in the brain, is associated with a gradual decline of cognitive abilities (for review, see [1]). Synaptic dysfunction and an imbalance between coordinated activities of different brain structures is hypothesized to be the main cause of abnormal functioning of the diseased brain [2 - 5]. Cognitive decline in AD is thought to be associated with alterations in synaptic transmission and thus in neuronal network function that is accompanied by modification of oscillations in the affected circuits [6, 7]. Superimposed extracellular fields arising from synaptic transmembrane currents of neurons involved in the circuits are supposed to form the electroencephalogram (EEG) [8] whose frequency composition has been shown to be associated with cognitive abilities of AD patients [9]. Substantial changes in the interhemispheric asymmetry in cortical EEG frequency spectra, demonstrated in AD patients [10], are in line with the well-known role of interhemispheric transfer for effective learning and memory [11]. Furthermore, changes in EEG recorded from the frontal cortex and/or the hippocampus, key brain areas in learning and memory processing, have been shown in an amyloid rat model of AD [12] and in numerous transgenic mouse models of AD [13 - 19].

Among transgenic mice, the 5xFAD line is distinguished by expressing multiple familial AD (FAD) mutations that additively increase amyloid-*beta*₄₂ ($A\beta_{42}$) production, the main hallmark in AD, and by causing dissociation between cortical and hippocampal synaptic plasticity [20], changes in cortical excitability and hippocampal rhythmicity, and defects in cholinergic transmission [18]. 5xFAD mice have been shown to exhibit intraneuronal $A\beta$ accumulation at 1.5 months, $A\beta$ deposition at 2 months, and memory deficits at 4 months of age [21] that are accompanied by defects in synaptic vesicle dynamics and neurotransmitter release [22]. Despite a significant $A\beta$ accumulation, the overall numbers of neurons in the frontal cortex and hippocampus in 5xFAD mice have been shown to equal those in age-matched controls, with the exception of a neuronal loss in cortical layer 5 [23]. Interestingly, before this specific structural dystrophy, synaptic deficits in layer 5 neurons were observed [24]. Thus, a deeper insight into the activities of different brain networks and their changes in the 5xFAD mice promises to aid effective analysis of the AD pathogenesis [18].

In a number of recent studies on AD transgenic mice (and 5xFAD, in particular), substantial attention has been paid to neuronal networks within/between the cortex and the hippocampus [12, 17 - 20, 25, 26]. Furthermore, the role of cholinergic, monoaminergic, and GABA-ergic transmission in the functioning of these networks has been shown [18, 25, 27]. In our previous study on an amyloid AD model, involvement of the dopaminergic (DA) system in the cortex-hippocampus EEG interplay has been revealed [12]. However, we are still lacking detailed information how this system is affected in the AD transgenic mice. This needs to be clarified

given data demonstrating a role of the DA system in both neuronal plasticity and amyloid-*beta* transformations in AD [28 - 30].

In this study on 5xFAD and non-transgenic (control) adult mice, we recorded EEGs from the secondary motor cortex, dorsal hippocampus, and from two DA-producing areas, the substantia nigra and ventral tegmental area, before and after systemic injection of a DA receptor agonist, apomorphine. Significant differences between 5xFAD and control mice were revealed in frequency spectra of both baseline and APO-evoked EEG activities in and between the brain areas.

2. Materials and Methods

Twelve six-month old male transgenic (Tg) mice with five familial AD mutations (5xFAD mice, B6SJL-Tg(APP^{Sw}FILon,PSEN1^{*M146L*L286V})6799Vas/J) were maintained on the C57BL/6J genetic background and fifteen non-transgenic (nTg, wild type control) littermates were used in this study. The 5xFAD mice were originally obtained from the Center for Collective Use of the Institute of Physiologically Active Compounds RAS (Chernogolovka, Russian Federation). Up to the age of five months, the mice were housed in groups of five per cage, while, thereafter, each of them was kept for 1.5 months in an individual cage. Mice were housed in a standard environment (12-h light/dark cycle, 22-25°C room temperature, 50-55% relative humidity) with food and water *ad libitum*. The procedures were carried out in accordance with the “Guidelines for accommodation and care of animals. Species-specific provisions for laboratory rodents and rabbits” (GOST 33216-2014) and in compliance with the principles enunciated in the Directive 2010/63/EU on the protection of animals used for scientific purposes, and approved by the local Institute Ethics Review Committee. All efforts were made to minimize both the number of the animals and their suffering.

All mice were genotyped using PCR analysis of DNA obtained from the ear/tail biopsy, followed by separation of the reaction products in the agarose gel. Mice with a transgene cassette in the genome were combined into Tg group, whereas those with lacking transgene were placed into nTg group. Post-mortem verification of the amyloid plaques in the brain slices (Suppl. 1), stained with thioflavin-S [32], revealed this AD hallmark in all mice from the Tg group.

2.1. Electrodes implantation and EEG recording

After one month of adaptation to the individual cage, each of six 5xFAD mice (29.7 ± 0.5 g) and nine nTg mice (33.0 ± 1.1 g) was anesthetized with subcutaneous (s.c.) injection of a combination of dissolved tiletamine/zolazepam (Zoletil®, Virbac, France) and xylazine solution (Rometa®, Bioveta, Czech Republic) at doses of 25 mg/kg and 2.5 mg/kg, respectively. Four recording electrodes were implanted into the left secondary motor cortex (MC; AP: +1.9, ML: -0.4, DV: -2.0), over the left dorsal hippocampus (HPC; AP: -2.8, ML: -2.7, DV: -1.7), into the left

ventral tegmental area (VTA; AP: -3.1, ML: -0.4, DV: -4.5), and into the right substantia nigra (SN; AP: -3.2, ML: +1.3, DV: -4.3) [33] (DV was measured from the skull surface). Within areas analyzed in this study, the opposite hemisphere for SN was chosen, firstly, because of its proximity to VTA which meant we could not exclude possible mutual damage during electrode implantation in the same hemisphere. Secondly, it is well known that the contralateral SN is the dominant source of DA in the opposite (here: left) hemisphere. Custom made electrodes were constructed from two varnish-insulated nichrom wires (100- μ m diameter) glued together (3M Vetbond™ Tissue Adhesive, MN, USA) with tips free from insulation for 100 μ m. Thus, prepared electrodes were sufficiently inflexible, and had higher effective surface/volume ratio than a mono-wire electrode of 200- μ m diameter. The reference and ground electrodes (stainless steel wire, 0.4 mm in diameter) were placed symmetrically into the caudal cavities behind the cerebrum (AP: -5.3, ML: \pm 1.8, DV: -0.5). All electrodes were positioned using a computerized 3D stereotaxic StereoDrive (Neurostar, Germany), fixed to the skull with dental cement and soldered to a dual row female connector (Sullins Connector Solutions, CA, USA). Both nichrom wires of the deep electrode were soldered to one of the connector's pins. After electrode implantation, animals were housed individually. *Post-mortem* verification of the electrode tip location included several steps: an anodal current (80-100 μ A, 1 s) coagulation of the adjacent tissue, extirpation of the brain and fixation of the cerebrum in 4% paraformaldehyde. The brain was cut in 30- μ m sections using a freezing microtome (Reicher, Austria). Coronal sections were examined to specify the electrode tip locations; EEG recordings from those, which did not meet placement criteria, were excluded from further analysis. Effective electrode targeting of the chosen brain areas was based on the use of the stereotaxic manipulator and on precise measurement of bregma and lambda coordinates. This high-tech manipulator allows the drilling of the holes for the electrodes exactly in the selected points on the skull. Precise estimations of an individual's bregma-lambda distance provides the correction of the coordinates for the brain areas, taking into account that the value used for preparation of the stereotaxic atlas [33] was equal to 4.2 ± 0.25 mm. In several cases, when the electrolytic marker was relatively enlarged, the electrode tip position was assigned to the point where the effect of electrolysis within the coagulated area was maximal. The frozen slices with the most effective electrode position were Nissl stained with cresyl violet acetate [34], magnified (Nikon Eclipse E200 microscope, Japan), digitized (DXM1200 camera, Japan), and used for illustration in combination with corresponding images of the mouse brain atlas [31] (Suppl. 2).

Three days after electrode implantation, each mouse was adapted for four days (1 h/day) to an experimental cage (Perspex, 15x17x20 cm) located in an electrically shielded chamber and to a cable (five 36-gauge wires, Plexon Inc, Texas, USA) plugged in a digital Neuro-MEP amplifier (Neurosoft Ltd, Ivanovo, Russian Federation). On day 8, a baseline EEG was recorded for 60 min, starting 20 min after placing the animal into the box. EEG recordings were continued for 120

minutes after s.c. injection either saline (control) or, on the next day, apomorphine (APO, Sigma, Milan, Italy), at a dose of 1.0 mg/kg. To minimize the effect of oxidation only freshly dissolved APO was used. All experiments were performed from 9 am to 6 pm in daylight combined with an artificial light source keeping illumination at a relatively stable level.

2.2. Computation of EEG frequency spectra

Monopolar EEG signals measured between the active and reference electrodes were amplified, filtered (0.1-35 Hz) and sampled (1 kHz) on-line using the amplifier and kept in memory of an operational computer for further analysis. The frequency spectra of successive 12-sec EEG epochs were studied using a modified version of period-amplitude analysis [35], which, in contrary to the Fourier transform, was not affected by well-known non-stationary nature of the EEG signals. The *absolute values* of the *half-wave* amplitudes with periods/frequencies in each of selected narrow EEG frequency subbands were summed followed by their normalization to the summarized values. In this study, twenty subbands in the 0.48 - 26.25 Hz range were analyzed: 0.48 - 0.53 (**0.5**), 0.87 - 0.97 (**0.9**), 1.29 - 1.43 (**1.4**), 1.74 - 1.92 (**1.8**), 2.21 - 2.44 (**2.3**), 2.71 - 3.0 (**2.9**), 3.25 - 3.59 (**3.4**), 3.82 - 4.22 (**4.0**), 4.44 - 4.91 (**4.7**), 5.12 - 5.66 (**5.4**), 5.86 - 6.48 (**6.2**), 6.68 - 7.38 (**7.0**), 7.59 - 8.39 (**8.0**), 8.63 - 9.54 (**9.1**), 9.83 - 10.86 (**10.3**), 11.25 - 12.43 (**11.8**), 12.98 - 14.35 (**13.7**), 15.21 - 16.82 (**16.0**), 18.36 - 20.3 (**19.3**), 23.75 - 26.25 (**25.0**). The subbands are marked in figures by their centre (mean) frequency values (see in brackets, above). The terms “lower” and “higher” in “classical” EEG bands *delta* (0.5 - 3.6 Hz), *theta* (3.8 - 8.4 Hz), *alpha* (8.6 - 12.4 Hz), and *beta* (12.9 - 26.2), are used below to differentiate corresponding frequency subbands of each band relative to its centre frequency (for more details, see [12]).

The frequency spectra of 12-sec EEG epochs were averaged for every successive 10-min interval for each mouse and for all of them separately from nTg and Tg groups. Relative differences in the averaged EEG spectra, obtained in the experiments with saline (day 1) and APO (day 2) in each group, were estimated as (APO - Saline) / Saline, in percentages, which providing the evaluation of APO effects in nTg and Tg groups.

2.3. Immunohistochemical techniques

In additional groups of 5xFAD and nTg mice (n = 6 in each group), the animals were deeply anaesthetized with ether and transcardially perfused consecutively with ice-cold saline and 4% paraformaldehyde in phosphate-buffered solution (PBS). Afterwards, the brains were promptly removed from the cranium and kept in the paraformaldehyde/PBS solution at 4°C for further histochemical analysis. For each animal, coronal brain sections (20-µm thick) at the level of VTA and SN were prepared using a freezing microtome (Reicher, Austria) and stored at -20°C in a cryoprotective solution (30% glycerol, 30% ethylene glycol in 0.05M PBS). To evaluate tyrosine hydroxylase (TH) immunoreactive cell populations in VTA and SN the slices were washed with

water and subsequently incubated overnight with rabbit polyclonal anti-TH antibodies (1:500, Chemicon, Woburn, MA, USA). Afterwards, they were incubated for one hour at room temperature with biotinylated goat secondary antibodies against rabbit's immunoglobulin (1:200, Abcam, UK) and with avidin-biotin-peroxidase complex (1:400, Sigma, USA). Peroxide content in the slices was measured after their incubation in a composition of 3,3'-diaminobenzidine-tetrahydrochloride (DAB; Sigma, St. Louis, USA) and H₂O₂ (at 0.05% and 0.02%, respectively) for 3-3.5 min at 20°C, followed by washing with PBS and fixation on gelatine-coated glass slides. Images of the brain slices were magnified (20x) and digitized (Nikon Eclipse E200 microscope and DXM1200 camera, respectively, Japan) for the count of the DA-producing neurons in the VTA and SN borders outlined using the atlas of TH-positive cells distribution [36]. The number of tyrosine hydroxylase immunopositive (TH+) cells was manually counted inside of symmetrical VTA and SN contours on each slide. Within thirty consecutive sections at the level of VTA and SN, five of them (every sixth one) were used for this analysis. Thus, the total statistics data were based on 2 x 5 x 6 = 60 contours of VTA or SN, meaning two symmetrical areas on one slide, five slides, and six animals, respectively. Averaged data obtained on ten contours per mouse were used in the final statistics on all animals.

The brain sections at the level of MC and HPC from the same mice were washed in PBS with Triton X100 and treated with H₂O₂ to inactivate endogenous peroxidase. They were consequently incubated with rabbit polyclonal anti-dopamine transporter antibody (MilliporeSigma, USA), with Biotin-conjugated goat secondary antibody (MilliporeSigma, USA), and, finally, with ExtraAvidin-Peroxidase (Sigma, USA), all diluted 1:300. After staining with DAB (Sigma, USA) and mounting on the pre-coated glass slides (Superfrost-plus Menzel, Germany), the slices were cover-slipped (Coverquick, Labonord, France) and analyzed at magnification of 20x using the microscope (Nikon E200, Japan). Dopamine transporter (DAT) levels were assessed symmetrically in both MC and HPC (the dentate gyrus, CA1-CA2, and CA3-CA4 areas) in five coronal sections (every sixth of thirty ones) per animal. Digitized images of 0.25 mm² in the target brain areas were analyzed by use of the Picture Analyzer Software, ImageJ, which estimated the DAB staining area. Averaged data obtained in ten 0.55 mm x 0.45 mm frames (0.25 mm²) per mouse were used in final statistics on all six animals.

2.4. Statistics

Differences in the averaged EEG spectra were evaluated by a two-tailed non-parametric Mann-Whitney U-test for individual frequency subbands, and by ANOVA for repeated measures when progression of EEG effects in the frequency ranges was analyzed either separately in different brain areas (one-way ANOVA) or between them (2-way ANOVA). Immunohistochemical data were analysed by a two-tailed non-parametric Mann-Whitney U-test with Bonferroni correction. The group data were expressed as the means ± SEM; differences were considered

significant at $p < 0.05$. For ANOVA and U-test analyses, STATISTICA 10 (StatSoft, Inc., Tulsa, OK, USA) was used, whereas power and effect size were calculated by use of G*Power 3.1.9.4 (www.psych.uni-duesseldorf.de/abteilungen/aap/gpower3). At the effect size of 0.75 - 0.9 and power of 0.8, G*Power showed that the sample sizes chosen for nTg and Tg groups (9 and 6 mice, respectively) were reasonable for our EEG study (see below).

3. Results

3.1. Baseline EEG from different brain areas

During baseline EEG recordings, both non-transgenic (nTg) and transgenic (Tg) 5xFAD mice were behaviorally active and characterized by intensive exploration of the experimental box that was very rarely (1-2/60 min) interrupted by short (< 60 sec) sleep-like bouts.

Baseline EEGs in freely moving and behaviourally active nTg and Tg (5xFAD) mice (Fig. 1 A and B, respectively) were characterized in MC and HPC by patterns of relatively slow (5 - 7 Hz) and very fast (14 - 25 Hz) oscillations. In the EEG from VTA, these patterns were also observed in Tg mouse, whereas powerful slow waves of 3 - 7 Hz were characteristic for nTg mouse. In the EEG from SN in nTg mouse, oscillations of 6 - 12 Hz predominated. The EEG patterns from MC and HPC were represented in their frequency spectra by peaks in *theta* and *beta* bands (Fig. 1, C, D). EEG spectra from VTA and SN in nTg mouse were characterized by wide peaks in the ranges of *theta* and *theta-alpha*, respectively, whereas, in Tg mouse, the peaks were found in the *lower theta* and *higher alpha-beta* (Fig. 1, E, F). These differences between the groups were stable in EEG spectra averaged over consecutive 10-min intervals and, thus, evidently observed in the spectral profiles that characterised the whole (60-min) baseline period (Fig. 2).

In 5xFAD mice, EEG activity in MC was enhanced during this period in both *delta* and *alpha* bands and suppressed in *beta* band, compared to those in nTg mice (Fig. 2, A; 2-way ANOVA for 15 samples x 6 repeats: $F_{1,78} > 15$, $p < 0.001$, for all bands). In HPC, the EEG differences in *delta* and *beta* bands *between the groups* were similar to those in MC (Fig. 2, B; 2-way ANOVA for 15 samples x 6 repeats: $F_{1,78} > 28$, $p < 0.001$, for both bands). In VTA of 5xFAD mice, relatively slow oscillations in *delta - theta* range were attenuated, whereas *beta* activity was enhanced, compared to those in nTg mice (Fig. 2, C; 2-way ANOVA for 15 samples x 6 repeats: $F_{1,78} > 34$, $p < 0.001$, for both frequency ranges). In SN (Fig. 2, D), significant differences between 5xFAD and nTg mice were observed in the same frequency ranges (2-way ANOVA for 15 samples x 6 repeats: $F_{1,78} > 24$, $p < 0.001$, for both ranges), however, the differences were evidently less than in VTA (c.f., Fig. 2, C and D, grey bars). All mentioned above differences were characterised by reasonable power and effect size measures (see Suppl. 3).

Averaged EEG frequency spectra in MC were identical to those in HPC in both groups of mice (Fig. 3, A). EEG differences between VTA and SN (Fig. 3, B), enhanced in *delta-theta* range and reduced in *beta* band in nTg mice, were diminished in 5xFAD mice (2-way ANOVA for 15

samples x 6 repeats: $F_{1,78} = 8.8$, $p < 0.01$ and $F_{1,78} = 6.3$, $p < 0.05$, for both frequency ranges). In nTg mice, EEG differences between VTA and MC (Fig. 3, C, dotted line), increased in *delta-alpha* range and decreased in *beta* band, were reduced in 5xFAD mice (Fig. 3, C, solid line) (2-way ANOVA for 15 samples x 6 repeats: $F_{1,78} > 270$, $p < 0.001$, for both frequency ranges). The profiles of relative differences between EEG spectra in SN and MC in nTg mice (Fig. 3, D, dotted line) were similar to those observed between VTA and MC. In 5xFAD mice, the EEG spectral differences between SN and MC (Fig. 3, D, solid line) were significantly diminished in *delta-alpha* range and in *beta* band (2-way ANOVA for 15 samples x 6 repeats: $F_{1,78} > 40$, $p < 0.001$, for both). All mentioned above differences were characterised by reasonable power and effect size measures (see Suppl. 4).

3.2. Apomorphine effects

After APO injection, behavioral reactions of both Tg and nTg mice were stereotyped: short-lasting freezing (1.5-2 min), followed by uninterrupted licking of the lower sides of the box that was accompanied by raising the tail. The behavioral response was comparable between Tg and nTg mice. Sleep-like bouts were very rare and short, and occurred at variable times.

In several pilot/supporting experiments on four nTg and three Tg mice, variations in EEG spectra after saline injections in two consecutive days were evaluated. In spite of visible scattered fluctuations in the EEG spectra averaged over consecutive 10-min intervals, no significant regularities in the frequency-time domain were observed (see Suppl. 5). Given these preliminarily obtained findings and obvious advantage of the experimenting on the same mouse, the sequence of saline and APO injections in day 1 and day 2, respectively, was chosen as preferable.

APO produced significant changes in *cortical* EEG activities in *delta* and *beta* bands (Fig. 4, A and B, respectively) compared to those observed after saline injection both in nTg mice (1-way ANOVA for 9 samples x 12 repeats: $F_{11,96} = 3.8$, $p < 0.001$ and $F_{11,95} = 2.6$, $p < 0.05$ for *delta* and *beta* bands, respectively) and in 5xFAD mice (1-way ANOVA for 6 samples x 12 repeats: $F_{11,60} = 3.3$, $p < 0.01$ and $F_{11,60} = 3.0$, $p < 0.01$, for *delta* and *beta* bands, respectively). APO-induced *delta* suppression and *beta* enhancement in the cortex were observed for 50 min after injection and both were more powerfully expressed in 5xFAD mice, compared to those in nTg mice (2-way ANOVA for 15 samples x 5 repeats: $F_{1,65} = 5.4$, $p < 0.05$ and $F_{1,65} = 9.8$, $p < 0.01$, for *delta* and *beta* bands, respectively). Similar APO effects revealed in *hippocampal* EEG (Fig. 4, C, D) evidently dominated for the whole 120-min period in 5xFAD mice over those in nTg mice in both *delta* and *beta* bands (2-way ANOVA for 15 samples x 12 repeats: $F_{1,156} = 15.2$, $p < 0.001$ and $F_{1,155} = 24.5$, $p < 0.001$, respectively). In EEG from VTA, APO suppressed *delta* activity for 50 minutes to a similar extent in both groups (Fig. 4, E; 2-way ANOVA for 15 samples x 12 repeats: $F_{1,156} = 0.8$, $p = 0.4$). In contrast, *beta* activity was significantly enhanced in 5xFAD mice compared to that in nTg mice (Fig. 4, F; 2-way ANOVA for 15 samples x 12 repeats: $F_{1,156} = 11.0$,

p < 0.01). The profiles of APO effect in SN (Fig. 4, G, H) were similar to those observed in VTA. The main differences between APO effects in nTg and Tg mice were predominantly observed for 50 minutes after APO injection and characterised by reasonable power and effect size measures (see Suppl. 6).

After APO injection, the main interregional differences between the groups were revealed in MC and VTA (Fig. 5). In nTg mice, APO suppressed *delta* activity in VTA for 50 min after injection to significantly higher extent than in MC (Fig. 5, A). In 5xFAD mice (Fig. 5, B), this difference was eliminated predominantly due to its enhancement in VTA (c.f., Fig. 5, A and B, black lines; 2-way ANOVA for 12 samples x 12 repeats: $F_{1,156} = 14.4$, $p < 0.001$). After APO injection, *beta* activity in MC was increased for 50 minutes in both nTg and 5xFAD mice (Fig. 5, C and D, respectively, grey lines). In nTg mice, APO produced phasic response in *beta* activity in VTA that was tended to be lower relative to that in MC (Fig. 5, C, black and grey lines, respectively). In 5xFAD mice, *beta* activity in VTA was significantly suppressed by APO, compared to that in MC (Fig. 5, D; 2-way ANOVA for 12 samples x 12 repeats: $F_{1,156} = 10.7$, $p < 0.01$). The differences in APO effects revealed in EEG from VTA and MC in nTg and Tg mice (Fig. 5, A and D, respectively) were characterised by reasonable power and effect size measures (see Suppl. 7).

3.3. DA cells and dopamine transporter (DAT) distribution

To investigate the impact of possible differences in the DA system in Tg and nTg mice on their EEG spectra, we stained brain sections with antibodies against TH or DAT at the levels of VTA-SN or MC-HPC areas, respectively (see Materials and Methods). The approaches revealed a significant decrease of both TH-positive (TH+) cells in the DA-producing areas and DAT vesicle density in the forebrain areas in 5xFAD mice (Fig. 6, A, C and B, D, respectively).

4. Discussion

In this study, we have shown significant differences between transgenic, 5xFAD, and non-transgenic (nTg), control, mice in *baseline* and *apomorphine-modified EEGs* recorded from different brain areas: secondary motor cortex (MC), hippocampus (HPC), ventral tegmental area (VTA), and substantia nigra (SN).

Baseline EEG

In baseline EEG from MC and HPC in 5xFAD mice, *delta* and *alpha* oscillations were more powerfully expressed than in nTg mice whereas those in *beta* band were suppressed (Fig. 2, A, B). The increase of *delta* waves in the EEGs recorded from MC and HPC in 5xFAD mice seems to be typical for transgenic murine AD models, as slower EEG activity has been shown in 5xFAD, TgCRND8, and APP single mutant mice [13, 16, 18]. The EEG alterations in transgenic mice are thought to be linked to the A β accumulation and plaque formation [17, 19]. However, EEG modifications associated with the *theta-gamma* coupling, in particular, have been shown in

transgenic mice to precede the excessive A β production and other AD features [16]. In adult 5xFAD mice, which have been shown to be characterized by typical AD indices (see, e.g., [21]), we demonstrate the slowing down of cortical and hippocampal oscillations in both *theta-delta* and *beta-alpha* ranges (Fig. 2, A, B). These effects seem to be associated with a significant suppression of DAT (Fig. 6, B, D) that might be expected to be associated with increase in DA in the synaptic cleft [37], which hypothetically is able to compensate, at least in part, for the loss of DA-producing neurones in VTA and SN (Fig. 6, A, C). The low level of DA receptor activation has been shown to be accompanied by EEG sleep features in the cortex [38]. Indeed, in 5xFAD mice, we observe a significant amplification of both *delta* and *alpha* oscillations in MC (Fig. 2, A), a hallmark of so-called "non-REM" sleep [39]. Transformation of *theta* and *beta* oscillations, which dominated in nTg mice, into a *delta* and *alpha* activities in 5xFAD mice suggesting the oscillatory circuits affected by excessive A β in transgenic mice have a potential for adaptive remodelling in response to the neurotoxicity of soluble A β [40], intraneuronal A β ₄₂-induced neurodegeneration and amyloid plaque formation, which are typical for 5xFAD mice [21]. Thus, further discovery of the mechanisms underlying reorganizing of disrupted neuronal circuits, involved, in particular, in sleep initiation might be useful for the development of a new therapeutic approach.

In EEG from VTA and SN in 5xFAD mice, averaged amplitudes of *delta-theta* waves were significantly decreased whereas those of *beta* rhythms were increased (Fig. 2, C, D). These frequency ranges coincide with those that characterise tonic (*delta-theta*) and so-called "bursting" (*beta*) neuronal activities in the DA-producing areas [41, 42]. Given these and an involvement of transmembrane currents in the origin of the EEG [8], the spectral differences in EEG from VTA and SN may be interpreted as a weakening of tonic spiking and strengthening of phasic bursting activity of DA neurones in 5xFAD mice. This is in line with an about four-fold higher rate of bursting patterns revealed in rats after long-term 6-hydroxydopamine lesions of DA neurons in SN [43]. The bias in profiles of VTA and SN neuronal activities is supposedly linked with DA cell loss in 5xFAD mice (Fig. 6, A, C). Evident correlation between the extent of DA cell loss in VTA (63%) and SN (48%), and *beta* activity increase in EEG from these areas (37% and 20%, respectively) in 5xFAD mice is in line with this suggestion (Fig. 2, C, D, grey bars in *beta* band). Partial DA cell loss is expected to invoke compensatory feed-back and feed-forward mechanisms [44]. Indeed, MC activation has been shown to initiate bursts in VTA neurons [45] effectively stimulating DA release in the cortex [46, 47]. This seems to be a vivid manifestation of a compensatory function of the MC-VTA networks in 5xFAD mice, which are characterized by depleted DAT in MC (Fig. 6, B, D) that is well known to initiate compensatory modifications in DA synapses [48].

In our study, the functioning of networks formed by different brain areas was evaluated through the relations between their EEG frequency spectra (Fig. 2). In mice from both groups, the relative spectral profiles of EEG from HPC and MC were flat (Fig. 3, A). Thus, the slowing of

EEGs from these areas in Tg mice (Fig. 2, A, B, grey bars) seems to be associated with synchronization of cortical and hippocampal oscillations that, in turn, may be correlated with the DAT level reduction observed in MC in 5xFAD mice (Fig. 6, B, D). Indeed, DA infusion into MC has been shown to produce a significant enhancement of EEG synchronization and/or coherence in MC and HPC [49]. Together, these suggest that DA transmission in the MC-HPC neuronal circuits in 5xFAD mice is unchanged.

In control mice, VTA recordings were characterized by increased *higher delta*-*lower theta* and decreased *lower alpha-beta* ranges (Fig. 2, C, grey line), that may be interpreted as a predominance of tonic discharges in VTA neurons and “bursting” activity in SN (see above). This specificity of DA-containing areas, revealed in their EEG spectral profiles, was lost in 5xFAD mice (Fig. 2, B, black line). Thus, the SN-VTA networks [50] in 5xFAD mice seem to be tuned to enhanced synchronization of the neuronal firing activity in the DA-producing nuclei. This is supposedly associated with the mechanisms, which are involved in the compensatory processes initiated by neuronal deficit in SN and VTA [51].

In 5xFAD mice, a significant attenuation of the spectral differences in EEG from DA nuclei and MC was observed throughout the analyzed frequency range (Fig. 3, C, D). Thus, the functional disturbances in 5xFAD mice seem to be predominantly associated with the attenuation of the oscillatory activity in their DA nuclei-forebrain networks.

Apomorphine effects

In control mice, APO produced a “desynchronising” effect in EEG from MC and HPC, with both attenuated *delta* and enhanced *beta* activities (Fig. 4, A - D, grey lines) similar to those observed in rats treated with APO at the same dose of 1.0 mg/kg [52]. At the lower dose of 0.01 mg/kg, APO has been shown to evoke EEG slowing biased to the *delta* range [38]. At high doses, APO activates postsynaptic DA receptors in terminal areas as DA release in the forebrain is completely blocked by APO at the level of the DA-producing nuclei through the activated autoreceptors [53]. Hence, a significant elevation of both suppression in *delta* band and activation in *beta* band in cortical and hippocampal EEG observed in 5xFAD mice (Fig. 4, A - D, black lines) might be explained by the increase in postsynaptic efficacy and/or enhanced sensitivity of DA receptors. Indeed, the neuronal population shrinkage in VTA and SN in 5xFAD mice (Fig. 6, A and C) is expected to result in chronic depletion of DA in the terminal areas of MC and HPC that in turn to initiate compensatory supersensitization of the postsynaptic DA receptors [54]. Similar APO effects in *delta* range of EEG from VTA and SN in mice from both groups (Fig. 4, E and G) underline a relatively high functional stability of basic mechanisms involved in tonic neuronal firing in these nuclei. On the other hand, significant differences revealed in *beta* (“bursting”) range in VTA and SN between 5xFAD and nTg mice (Fig. 4, F and H) seem to be associated with the feed-back effects of the APO-activated forebrain on the DA-producing neurons in an attempt to compensate for their APO-suppressed bursting activity [45].

APO effects on the EEG spectra in mice from different groups are expressed in both frequency and brain area specific manner (Fig. 5) that might be associated with differences in regional sensitivity of DA receptors to APO. Indeed, *delta* activity, slightly suppressed by APO in MC of mice from both groups (Fig. 5, A, B, grey lines), is roughly affected by APO in VTA, while at lower extent in 5xFAD mice (Fig. 5, A, B, black lines). In contrast, APO enhancing of cortical *beta* activity, comparable in mice from both groups (Fig. 5, C, D, grey lines), is accompanied by a significant *beta* suppression in VTA, predominantly in 5xFAD mice (Fig. 5, C, D, black lines). Given the deficit of DA-producing neurones in 5xFAD mice (Fig. 6, A, C) these results might be concluded to be consistent with the suggestion that DA-ergic deprivation is accompanied by hypersensitization of post- and pre-synaptic DA receptors [54, 55]. Furthermore, the significant *amplification* of APO-induced *delta* activity in EEG from VTA in 5xFAD mice (c.f. Fig. 5, A and B, black lines) is seemingly associated with sensitization of post-synaptic receptors whereas the *beta attenuation* (c.f. Fig. 5, C and D, black lines) may be due to the pre-synaptic modifications. The differences revealed in APO effects on EEG from VTA in 5xFAD and nTg mice and similarities of those in MC (Fig. 5) might be explained by a regional selectivity of DA clearing mechanisms associated with predominant activity of either DAT or catechol-o-methyltransferase (in MC, in particular) [56]. Characteristic DAT levels in MC and DG, different in nTg mice and similar in Tg mice (Fig. 6, D), are indirectly consistent with this suggestion. DAT activity deficit is expected could be accompanied by an increase of DA level in the synaptic clefts that in turn might initiate a compensatory desensitization of both pre- and post-synaptic DA receptors [48]. Thus, the deficit of both DA-producing neurones and DAT in 5xFAD mice might be suggested to affect the DA receptors sensitivity resulting in compensatory reorganization of the neuronal networks in/within various brain areas. This is expected could lead to modifications of the APO effects on the EEG oscillations generated by the affected networks.

In conclusion, the links between EEG spectra modifications and various intracerebral network transformations in the transgenic model of familial AD, 5xFAD mice, are analyzed in this work. We have shown that EEGs from dopamine-containing areas in the midbrain and in their terminal forebrain structures are altered in these animals. Associations of these alterations with shrinkage of DA-producing cell population, lowered dopamine transporter level, and modified sensitivity of dopamine receptors, which were revealed in this study, are discussed. We suggest that this EEG approach might be a useful tool for further studies of the adaptive/compensatory neuronal network remodelling associated with disturbances in the dopaminergic system. Regardless of the sources of these disturbances, in particular, associated with α -synuclein involvement [57], they are expected to shift the balance between neurogenesis [58] and senescence [59] towards the later, resulting in the neurodegenerative pathology.

Acknowledgment: This work was supported by Grant RSF 18-15-00392.

Animals were supported by the budget of the IPAC RAS State Targets topic # 0090-2019-0005.

457 **Conflict of interest:** The authors declare that they have no conflict of interest.
458

References

- [1] Hampel H, Mitchell A, Blennow K, Frank RA, Brettschneider S, Weller L, Moller HJ (2004) Core biological marker candidates of Alzheimer's disease - perspectives for diagnosis, prediction of outcome and reflection of biological activity. *J Neural Transm* **111**(3), 247-272.
- [2] Selkoe DJ (2002) Alzheimer's disease is a synaptic failure. *Science* **298**(5594), 789-791.
- [3] Vorobyov V, Sengpiel F (2008) Apomorphine-induced differences in cortical and striatal EEG and their glutamatergic mediation in 6-hydroxydopamine-treated rats. *Exp Brain Res* **191**, 277-287.
- [4] Oswal A, Brown P, Litvak V (2013) Synchronized neural oscillations and the pathophysiology of Parkinson's disease. *Curr Opin Neurol* **26**, 662-670.
- [5] Tampellini D (2015) Synaptic activity and Alzheimer's disease: a critical update. *Front Neurosci* **9**, 423. doi: 10.3389/fnins.2015.00423. eCollection 2015.
- [6] Nimrich V, Draguhn A, Axmacher N (2015) Neuronal Network Oscillations in Neurodegenerative Diseases. *Neuromolecular Med* **17**(3), 270-284.
- [7] Palop JJ, Mucke L (2016) Network abnormalities and interneuron dysfunction in Alzheimer disease. *Nat Rev Neurosci* **17**(12), 777-792.
- [8] Buzsáki G, Anastassiou CA, Koch C (2012) The origin of extracellular fields and currents-- EEG, ECoG, LFP and spikes. *Nat Rev Neurosci* **13**(6), 407-420.
- [9] Koenig T, Prichet L, Dierks T, Hubl D, Wahlund LO, John ER, Jelic V (2005) Decreased EEG synchronization in Alzheimer's disease and mild cognitive impairment. *Neurobiol Aging* **26**(2), 165-171.
- [10] Lakmache Y, Lassonde M, Gauthier S, Frigon JY, Lepore F (1998) Interhemispheric disconnection syndrome in Alzheimer's disease. *Proc Natl Acad Sci USA* **95**(15), 9042-9046.
- [11] Davidson RJ (2004) What does the prefrontal cortex "do" in affect: perspectives on frontal EEG asymmetry research. *Biol Psychol* **67**(1-2), 219-233.
- [12] Vorobyov V, Kaptsov V, Gordon R, Makarova E, Podolski I, Sengpiel F (2015) Neuroprotective effects of hydrated fullerene C60: cortical and hippocampal EEG interplay in an amyloid-infused rat model of Alzheimer's disease. *J Alzheimer's Dis* **45**, 217-233.
- [13] Wang J, Ikonen S, Gurevicius K, van Groen T, Tanila H (2002) Alteration of cortical EEG in mice carrying mutated human APP transgene. *Brain Res* **943**(2), 181-190.
- [14] Cissé M, Sanchez PE, Kim DH, Ho K, Yu GQ, Mucke L (2011) Ablation of cellular prion protein does not ameliorate abnormal neural network activity or cognitive dysfunction in the J20 line of human amyloid precursor protein transgenic mice. *J Neurosci* **31**(29), 10427-10431.
- [15] Scott L, Kiss T, Kawabe TT, Hajós M (2016) Neuronal network activity in the hippocampus of tau transgenic (Tg4510) mice. *Neurobiol Aging* **37**, 66-73.

- [16] Goutagny R, Gu N, Cavanagh C, Jackson J, Chabot JG, Quirion R, Krantic S, Williams S (2013) Alterations in hippocampal network oscillations and *theta-gamma* coupling arise before A β overproduction in a mouse model of Alzheimer's disease. *Eur J Neurosci* **37**(12), 1896-1902.
- [17] Schneider F, Baldauf K, Wetzel W, Reymann KG (2014) Behavioral and EEG changes in male 5xFAD mice. *Physiol Behav* **135**, 25-33.
- [18] Siwek ME, Müller R, Henseler C, Trog A, Lundt A, Wormuth C, Broich K, Ehninger D, Weiergräber M, Papazoglou A (2015) Altered *theta* oscillations and aberrant cortical excitatory activity in the 5XFAD model of Alzheimer's disease. *Neural Plast* **781731**. doi: 10.1155/2015/781731.
- [19] Scott L, Feng J, Kiss T, Needle E, Atchison K, Kawabe TT, Milici AJ, Hajós-Korcsok E, Riddell D, Hajós M (2012) Age-dependent disruption in hippocampal θ oscillation in amyloid- β overproducing transgenic mice. *Neurobiol Aging* **33**(7), 1481.e13-23, doi: 10.1016/j.neurobiolaging.2011.12.010.
- [20] Crouzin N, Baranger K, Cavalier M, Marchalant Y, Cohen-Solal C, Roman FS, Khrestchatsky M, Rivera S, Féron F, Vignes M (2013) Area-specific alterations of synaptic plasticity in the 5XFAD mouse model of Alzheimer's disease: dissociation between somatosensory cortex and hippocampus. *PLoS One* **8**(9), e74667. doi: 10.1371/journal.pone.0074667. eCollection 2013.
- [21] Oakley H, Cole SL, Logan S, Maus E, Shao P, Craft J, Guillozet-Bongaarts A, Ohno M, Disterhoft J, Van Eldik L, Berry R, Vassar R (2006) Intraneuronal β -amyloid aggregates, neurodegeneration, and neuron loss in transgenic mice with five familial Alzheimer's disease mutations: potential factors in amyloid plaque formation. *J Neurosci* **26**(40), 10129–10140.
- [22] Marsh SE, Blurton-Jones M (2012) Examining the mechanisms that link β -amyloid and α -synuclein pathologies. *Alzheimers Res Ther* **4**(2), 11. doi: 10.1186/alzrt109. eCollection 2012.
- [23] Jawhar S, Trawicka A, Jenneckens C, Bayer TA, Wirths O (2012) Motor deficits, neuron loss, and reduced anxiety coinciding with axonal degeneration and intraneuronal A β aggregation in the 5XFAD mouse model of Alzheimer's disease. *Neurobiol Aging* **33**(1), 196.e29-40 doi: 10.1016/j.neurobiolaging.2010.05.027.
- [24] Buskila Y1, Crowe SE, Ellis-Davies GC (2013) Synaptic deficits in layer 5 neurons precede overt structural decay in 5xFAD mice. *Neuroscience* **254**, 152-159.
- [25] Rubio SE, Vega-Flores G, Martínez A, Bosch C, Pérez-Mediavilla A, del Río J, Gruart A, Delgado-García JM, Soriano E, Pascual M (2012) Accelerated aging of the GABAergic septohippocampal pathway and decreased hippocampal rhythms in a mouse model of Alzheimer's disease. *FASEB J* **26**(11), 4458-4467.
- [26] Paesler K, Xie K, Hettich MM, Siwek ME, Ryan DP, Schröder S, Papazoglou A, Broich K, Müller R, Trog A, Garthe A, Kempermann G, Weiergräber M, Ehninger D (2015) Limited effects

of an eIF2 α S51A allele on neurological impairments in the 5xFAD mouse model of Alzheimer's disease. *Neural Plast* **825157**, doi: 10.1155/2015/825157.

[27] Dringenberg HC (2000) Alzheimer's disease: more than a 'cholinergic disorder' - evidence that cholinergic-monoaminergic interactions contribute to EEG slowing and dementia. *Behav Brain Res* **115**(2), 235-249.

[28] Koch G, Esposito Z, Codecà C, Mori F, Kusayanagi H, Monteleone F, Di Lorenzo F, Bernardi G, Martorana A (2011) Altered dopamine modulation of LTD-like plasticity in Alzheimer's disease patients. *Clin Neurophysiol* **122**(4), 703-707.

[29] Himeno E, Ohyagi Y, Ma L, Nakamura N, Miyoshi K, Sakae N, Motomura K, Soejima N, Yamasaki R, Hashimoto T, Tabira T, LaFerla FM, Kira J (2011) Apomorphine treatment in Alzheimer mice promoting amyloid- β degradation. *Ann Neurol* **69**(2), 248-256.

[30] Lu J, Li X, Wang Q, Pei G (2017) Dopamine D2 receptor and β -arrestin 2 mediate Amyloid- β elevation induced by anti-parkinson's disease drugs, levodopa and piribedil, in neuronal cells. *PLoS One* **12**(3), e0173240. doi: 10.1371/journal.pone.0173240.

[31] Rosen GD, Williams AG, Capra JA, Connolly MT, Cruz B, Lu L, Airey DC, Kulkarni K, Williams RW (2000) The Mouse Brain Library @ www.mbl.org. Int Mouse Genome Conference 14: 166. www.mbl.org.

[32] Bussi re T, Bard F, Barbour R, Grajeda H, Guido T, Khan K, Schenk D, Games D, Seubert P, Buttini M (2004) Morphological characterization of Thioflavin-S-positive amyloid plaques in transgenic Alzheimer mice and effect of passive A β immunotherapy on their clearance. *Am J Pathol* **165**(3), 987-995.

[33] Franklin KBJ, Paxinos G (2007) The Mouse Brain in Stereotaxic Coordinates. Third edition Academic Press, New York, USA.

[34] Gerfen CR (2003) Basic Neuroanatomical Methods. *Current Protocols in Neuroscience* 00:1.1:1.1.1–1.1.11. doi: 10.1002/0471142301.ns0101s23, John Wiley & Sons.

[35] Gal'chenko AA, Vorobyov VV (1999) Analysis of electroencephalograms using a modified amplitude-interval algorithm. *Neurosci Behav Physiol* **29**, 157-160.

[36] H kfelt T, Martensson R, Bj rklund A, Kheinau S, Goldstein M (1984) In Bj rklund A, H kfelt T. (Eds.), *Handbook of Chemical Neuroanatomy*. Elsevier Science B.V, Amsterdam, Part 1, Vol. 2, pp. 277-379.

[37] Sotnikova TD, Beaulieu JM, Gainetdinov RR, Caron MG (2006) Molecular biology, pharmacology and functional role of the plasma membrane dopamine transporter. *CNS Neurol Disord Drug Targets* **5**, 45–56.

[38] Sebban C, Zhang XQ, Tesolin-Decros B, Millan MJ, Spedding M (1999) Changes in EEG spectral power in the prefrontal cortex of conscious rats elicited by drugs interacting with dopaminergic and noradrenergic transmission. *Br J Pharmacol* **128**(5), 1045-1054.

566 [39] Vyazovskiy VV, Achermann P, Borbély AA, Tobler I (2004) The dynamics of spindles and
567 EEG slow-wave activity in NREM sleep in mice. *Arch Ital Biol* **142**(4), 511-523.

568 [40] Mucke L, Selkoe DJ (2012) Neurotoxicity of amyloid β -protein: synaptic and network
569 dysfunction. Cold Spring Harb. *Perspect Med* **2**(7), a006338. doi: 10.1101/cshperspect.a006338.

570 [41] Paladini CA, Roeper J (2014) Generating bursts (and pauses) in the dopamine midbrain
571 neurons. *Neuroscience* **282**, 109-121.

572 [42] Hage TA, Khaliq ZM (2015) Tonic firing rate controls dendritic Ca^{2+} signaling and synaptic
573 gain in substantia nigra dopamine neurons. *J Neurosci* **35**(14), 5823-5836.

574 [43] Seeger-Armbruster S, von Ameln-Mayerhofer A (2013) Short- and long-term unilateral 6-
575 hydroxydopamine lesions in rats show different changes in characteristics of spontaneous firing
576 of substantia nigra pars reticulata neurons. *Exp Brain Res* **224**(1), 15-24.

577 [44] Duda J, Pötschke C, Liss B (2016) Converging roles of ion channels, calcium, metabolic
578 stress, and activity pattern of Substantia nigra dopaminergic neurons in health and Parkinson's
579 disease. *J Neurochem* **139** Suppl 1, 156-178.

580 [45] Tong ZY, Overton PG, Clark D (1996) Antagonism of NMDA receptors but not AMPA/kainate
581 receptors blocks bursting in dopaminergic neurons induced by electrical stimulation of the
582 prefrontal cortex. *J Neural Transm* **103**, 889-904.

583 [46] Au-Young SM, Shen H, Yang CR (1999) Medial prefrontal cortical output neurons to the
584 ventral tegmental area (VTA) and their responses to burst-patterned stimulation of the VTA:
585 neuroanatomical and in vivo electrophysiological analyses. *Synapse* **34**(4), 245-255.

586 [47] Sesack SR, Grace AA (2010) Cortico-basal ganglia reward network: microcircuitry.
587 *Neuropsychopharmacology* **35**, 27-47.

588 [48] Lohr KM, Masoud ST, Salahpour A, Miller GW (2017) Membrane transporters as mediators
589 of synaptic dopamine dynamics: implications for disease. *Eur J Neurosci* **45**(1), 20-33.

590 [49] Benchenane K, Peyrache A, Khamassi M, Tierney PL, Gioanni Y, Battaglia FP, Wiener SI
591 (2010) Coherent *theta* oscillations and reorganization of spike timing in the hippocampal -
592 prefrontal network upon learning. *Neuron* **66**(6), 921-936.

593 [50] Ferreira JG, Del-Fava F, Hasue R.H, Shammah-Lagnado SJ (2008) Organization of ventral
594 tegmental area projections to the ventral tegmental area-nigral complex in the rat. *Neuroscience*
595 **153**(1), 196-213.

596 [51] Golden JP, Demaro JA 3rd, Knoten A, Hoshi M, Pehek E, Johnson EM Jr, Gereau RW 4th,
597 Jain S (2013) Dopamine-dependent compensation maintains motor behavior in mice with
598 developmental ablation of dopaminergic neurons. *J Neurosci* **33**(43), 17095-17107.

599 [52] Gessa GL, Porceddu ML, Collu M, Mereu G, Serra M, Ongini E, Biggio G (1985) Sedation
600 and sleep induced by high doses of apomorphine after blockade of D-1 receptors by SCH 23390.
601 *Eur J Pharmacol* **109**(2), 269-274.

- [53] Zetterström T, Ungerstedt U (1984) Effects of apomorphine on the in vivo release of dopamine and its metabolites, studied by brain dialysis. *Eur J Pharmacol* **97**(1-2), 29-36.
- [54] Kostrzewa RM, Kostrzewa JP, Brown RW, Nowak P, Brus R (2008) Dopamine receptor supersensitivity: development, mechanisms, presentation, and clinical applicability. *Neurotox Res* **14**, 121–128.
- [55] Robinson S, Smith DM, Mizumori SJ, Palmiter RD (2004) Firing properties of dopamine neurons in freely moving dopamine-deficient mice: effects of dopamine receptor activation and anesthesia. *Proc Natl Acad Sci USA* **101**(36), 13329-13334.
- [56] Cockerham R, Liu S, Cachope R, Kiyokage E, Cheer JF, Shipley MT, Puche AC (2016) Subsecond Regulation of Synaptically Released Dopamine by COMT in the Olfactory Bulb. *J Neurosci* **36**(29), 7779-7785.
- [57] Garcia-Reitboeck P, Anichtchik O, Dalley JW, Ninkina N, Tofaris GK, Buchman VL, Spillantini MG (2013) Endogenous *alpha*-synuclein influences the number of dopaminergic neurons in mouse substantia nigra. *Exp Neurol* **248**, 541-545.
- [58] Höglinger GU, Rizk P, Muriel MP, Duyckaerts C, Oertel WH, Caille I, Hirsch EC (2004) Dopamine depletion impairs precursor cell proliferation in Parkinson disease. *Nat Neurosci* **7**(7), 726-735.
- [59] Nekrasov PV, Vorobyov VV (2018) Dopaminergic mediation in the brain aging and neurodegenerative diseases: a role of senescent cells. *Neural Regen Res* **13**(4), 649-650.

Figures legends

Figure 1. Typical patterns in 12-s fragments of baseline EEG in wakeful and behaviourally active non-transgenic (nTg) and 5xFAD (Tg) mice (**A** and **B**, respectively) and their frequency spectra (**C** - **F**) in the secondary motor cortex (MC), hippocampus (HPC), and the nuclei containing DA-synthesizing neurons: substantia nigra (SN) and ventral tegmental area (VTA).

On **A** and **B**, time calibration is 1 sec, amplitude calibration is 100 μ V. On **C** - **F**, abscissa is a frequency subband marked with its mean value, in hertz; ordinate is summed amplitudes of EEG in each of 20 subbands, normalized to a sum of all amplitude values, in arbitrary units. Alternating white and grey bars indicate "classical" EEG frequency bands (from left to right): *delta*, *theta*, *alpha*, and *beta*.

Figure 2. Averaged amplitude-frequency spectra of 12-s baseline EEG fragments recorded from MC (**A**), HPC (**B**), VTA (**C**), and SN (**D**) for 60 min in non-transgenic (nTg, n = 9) and 5xFAD (Tg, n = 6) mice (dashed and solid lines, respectively) and spectral ratios (narrow grey bars) between the groups (Tg/nTg).

Abscissa is a frequency subband marked with its mean value, in hertz; the left ordinate is summed absolute values of EEG amplitudes in each of 20 subbands, normalized to sum of all amplitude values, in arbitrary units; the right ordinate is a ratio of the EEG amplitudes, calculated as (Tg - nTg) / nTg, in %. Vertical lines are ± 1 SEM; diamond denotes a significant difference between the groups ($p < 0.05$, Wilcoxon test). Alternating white and grey bars indicate "classical" EEG frequency bands (from left to right): *delta*, *theta*, *alpha*, and *beta*.

Figure 3. Relations between averaged amplitude-frequency spectra of 12-s baseline EEG fragments recorded from the secondary motor cortex (MC), superficial layers of the hippocampal CA1 area (HPC), substantia nigra (SN), and ventral tegmental area (VTA) for 60 min in non-transgenic (nTg, n = 9) and 5xFAD (Tg, n = 6) mice (dashed and solid lines, respectively). Abscissa is a frequency subband marked with its mean value in hertz; ordinate is a ratio of summed absolute values of baseline EEG amplitudes in each of 20 subbands, normalized to sum of all amplitudes of EEG recorded from different brain areas, calculated as (Area 1 - Area 2) / Area 2, in %, characterizing genetically determined EEG relations between them. Vertical lines are ± 1 SEM; diamond denotes a significant difference between the groups ($p < 0.05$, Wilcoxon test). Alternating white and grey bars indicate "classical" EEG frequency bands (from left to right): *delta*, *theta*, *alpha*, and *beta*.

Figure 4. Evolution of apomorphine (APO, 1.0 mg/kg, s.c.) vs. saline effects in *delta* and *beta* frequency bands (**A**, **C**, **E**, **G** and **B**, **D**, **F**, **H**, respectively) of EEG from MC, HPC, VTA, and SN in non-transgenic (nTg, n = 9) and 5xFAD (Tg, n = 6) mice (gray and black lines, respectively).

Abscissa shows time after injection, marked in 10-min intervals. Ordinate is a ratio of the averaged EEG amplitudes in the indicated frequency bands, obtained in experiments with saline and APO in each group, and estimated as $(\text{APO} - \text{Saline}) / \text{Saline}$, in %, characterizing APO effects in nTg and Tg groups. A difference between baseline EEG ratios in Tg and nTg mice was used for normalization of APO effects in Tg group. Diamond denotes a significant difference between the groups ($p < 0.05$, Wilcoxon test). Error bars show ± 1 SEM.

Figure 5. Evolution of apomorphine (APO, 1.0 mg/kg, s.c.) effects in *delta* and *beta* bands of EEG from MC and VTA in non-transgenic (nTg) and 5xFAD mice ($n = 9$ and 6 , respectively). Abscissa shows time after APO injection, marked in 10-min intervals. Ordinate is EEG amplitudes (in arbitrary units) summed in the indicated frequency bands in different brain areas separately for each group and normalized to EEG baseline values in MC (horizontal dashed lines). Diamond denotes a significant difference between the groups ($p < 0.05$, Wilcoxon test). Error bars show ± 1 SEM.

Figure 6. Distribution of tyrosine hydroxylase immunopositive (TH+) cells (**A, C**) and dopamine transporter (DAT) (**B, D**) in different brain areas in non-transgenic (nTg) and transgenic (Tg, 5xFAD) mice. On **A**, photomicrographs from nTg (**a, b**) and Tg (**c, d**) experimental mice display TH+ cells (black pyramids) in the ventral tegmental area (VTA) and the substantia nigra (SN), outlined by dashed ellipsis on the centered section, modified from [31]. On **B**, photomicrographs display DAT vesicles distributions (black spots) in the dentate gyrus (DG) from nTg (**a**) and Tg (**b**) experimental mice in the area outlined by open white rectangle. Obvious loss of TH-positive neurons and DAT vesicles is observed in 5xFAD mice. Horizontal white bars on **A** and **B** denote the scales of $50 \mu\text{m}$. On **C**, abscissa demonstrates the brain areas with DA-producing neurons, VTA and SN; on **D**, abscissa shows the brain areas containing DAT: MC, DG, and hippocampal CA1-CA2, and CA3-CA4 fields. Ordinate on **C** is the number of TH-positive cells in the boundaries of VTA and SN; ordinate on **D** is the DAT-containing area (in mm^2), accounted in the frame of $0.55 \text{ mm} \times 0.45 \text{ mm}$ (0.25 mm^2). Stars denote significant differences between Tg and nTg groups, ** – $p < 0.01$, *** – $p < 0.001$ (two-tailed U-test).

Baseline EEG fragments and their frequency spectra

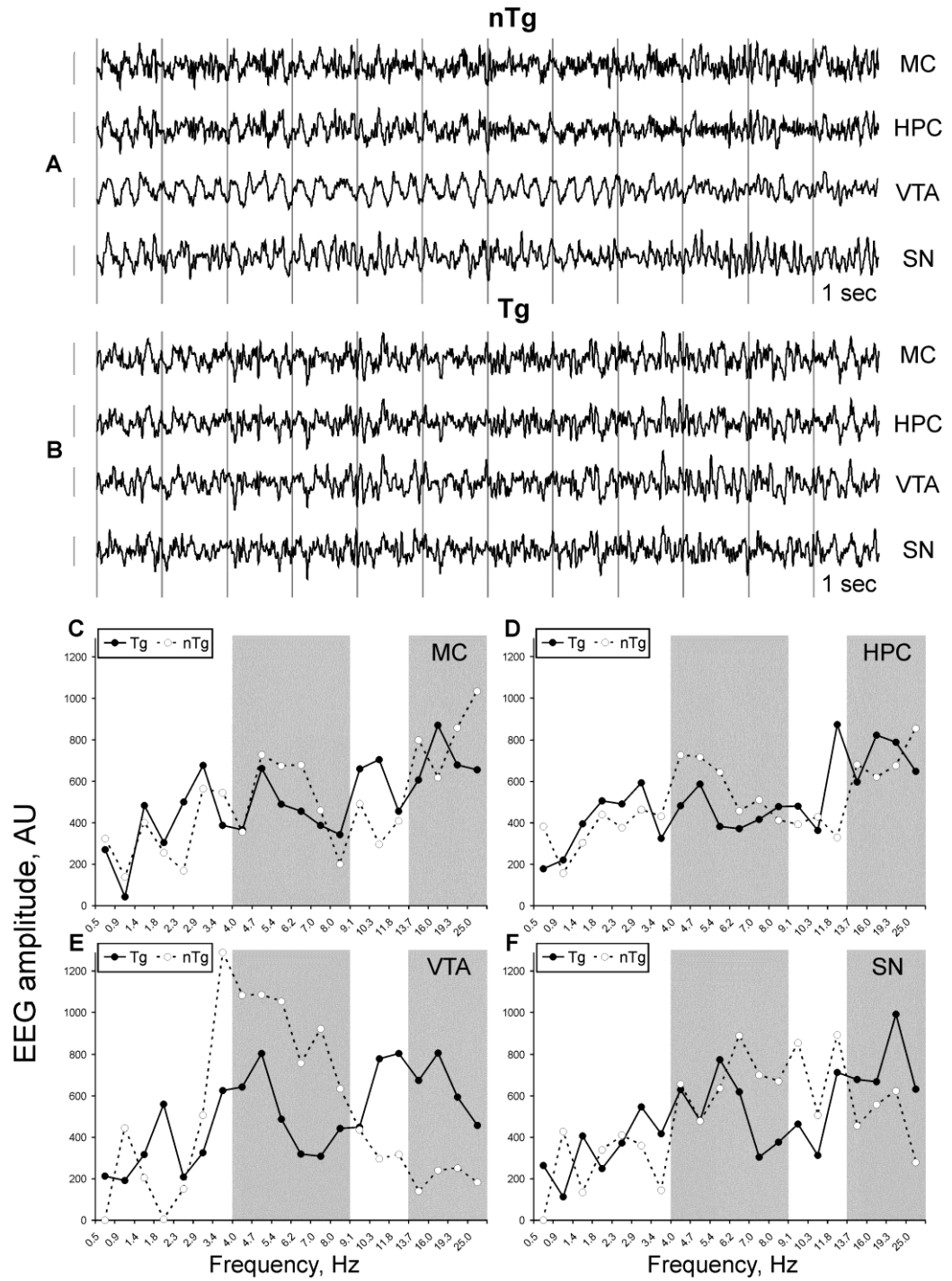


Figure 1

Averaged baseline EEG spectra in 5xFAD vs. non-transgenic mice

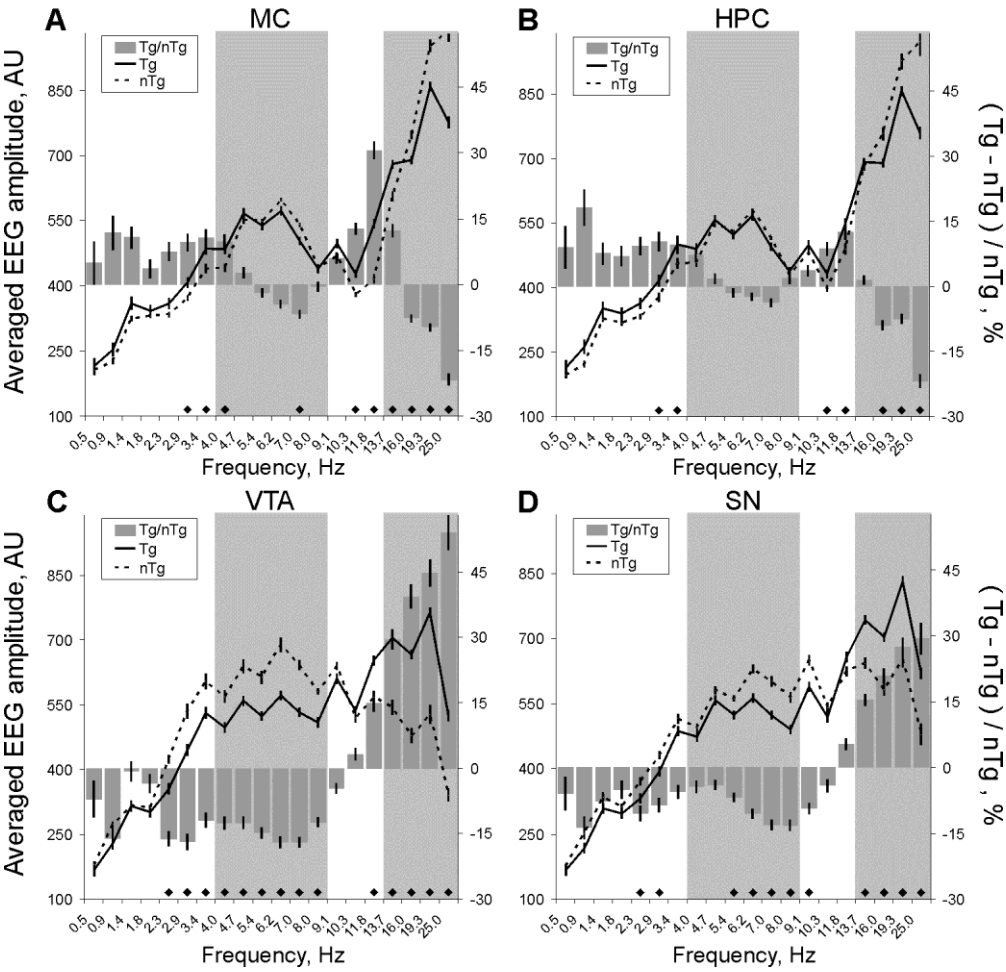


Figure 2

Baseline EEG relations between the brain areas in mice from different groups

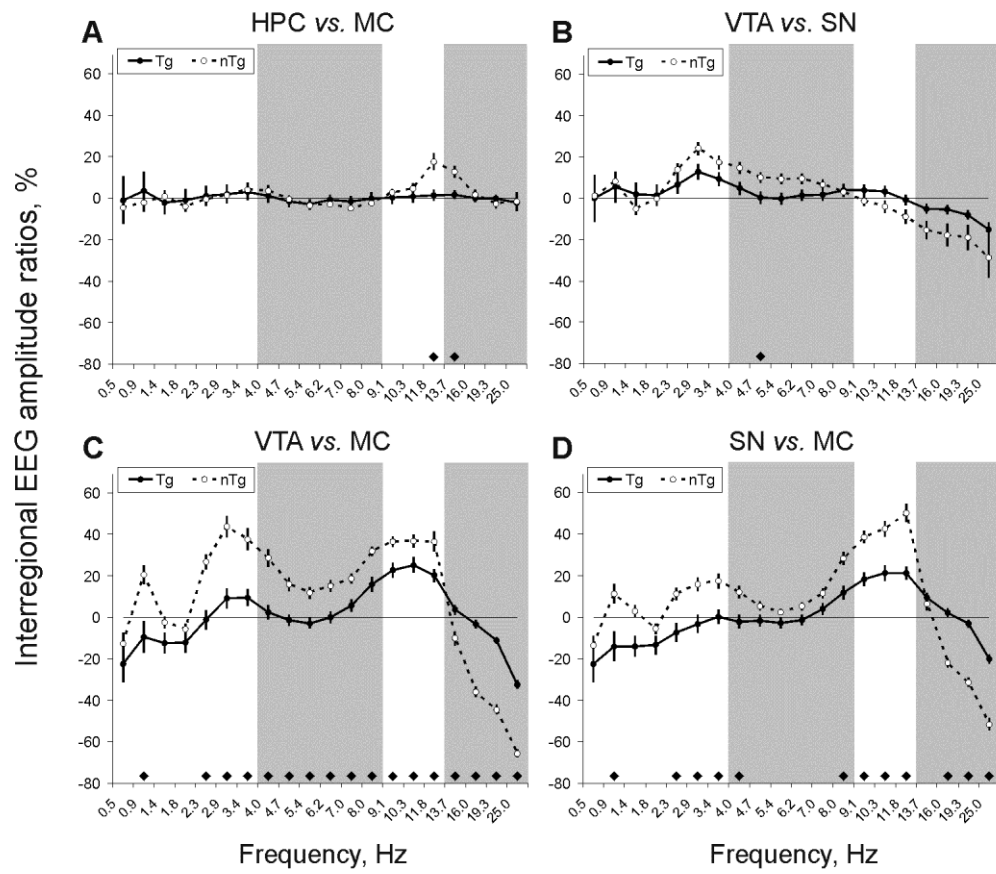
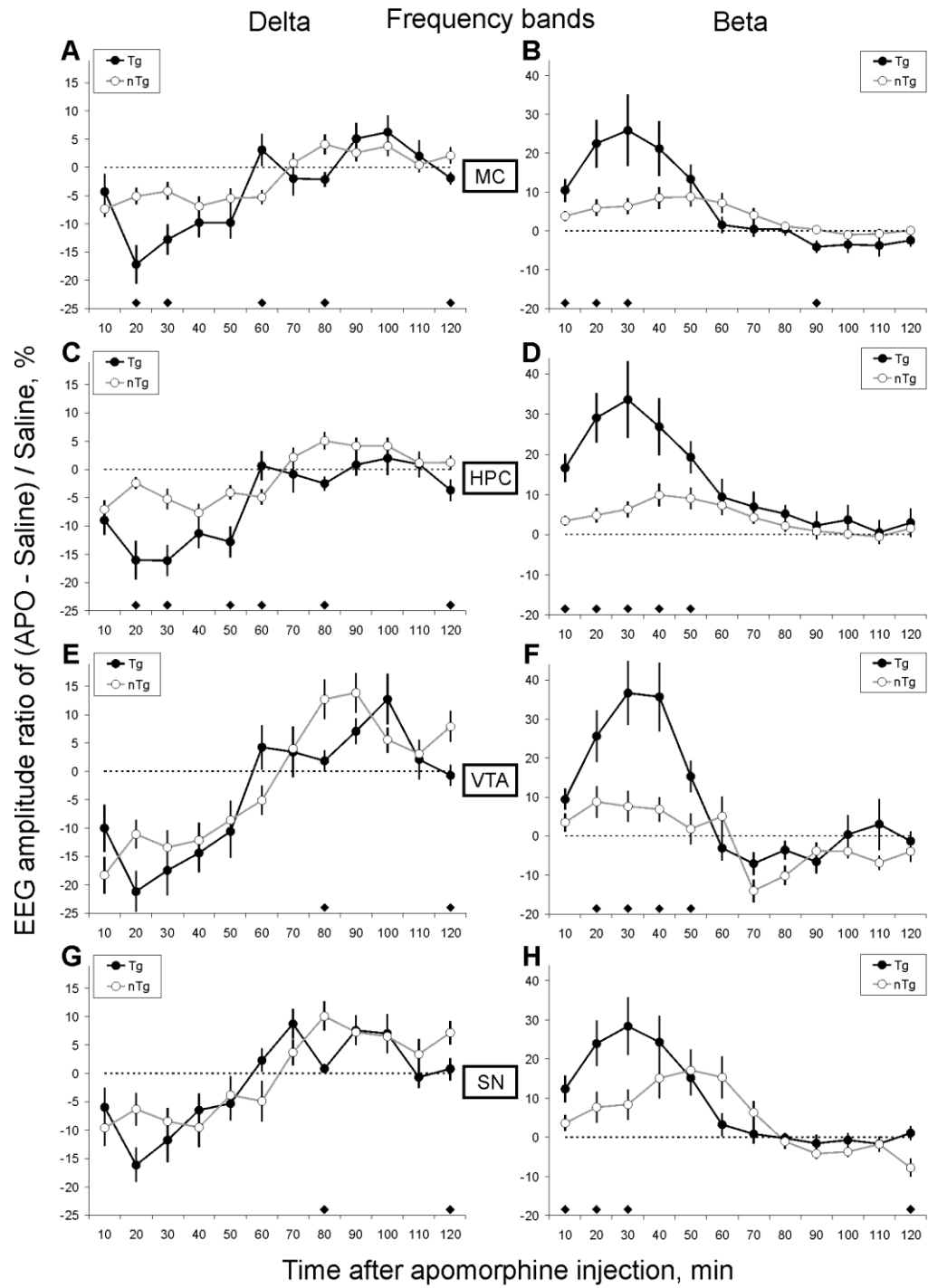


Figure 3

EEG effects of APO vs. saline in 5xFAD and control mice



APO effects in EEG from MC and VTA in mice from different groups

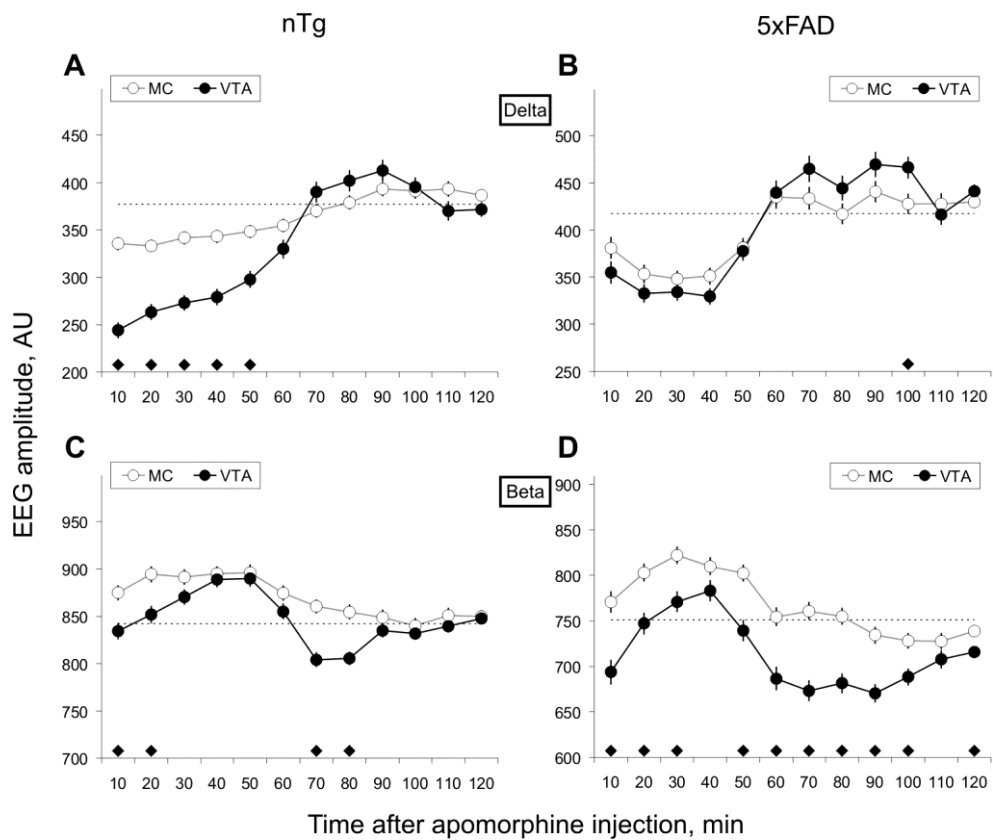


Figure 5

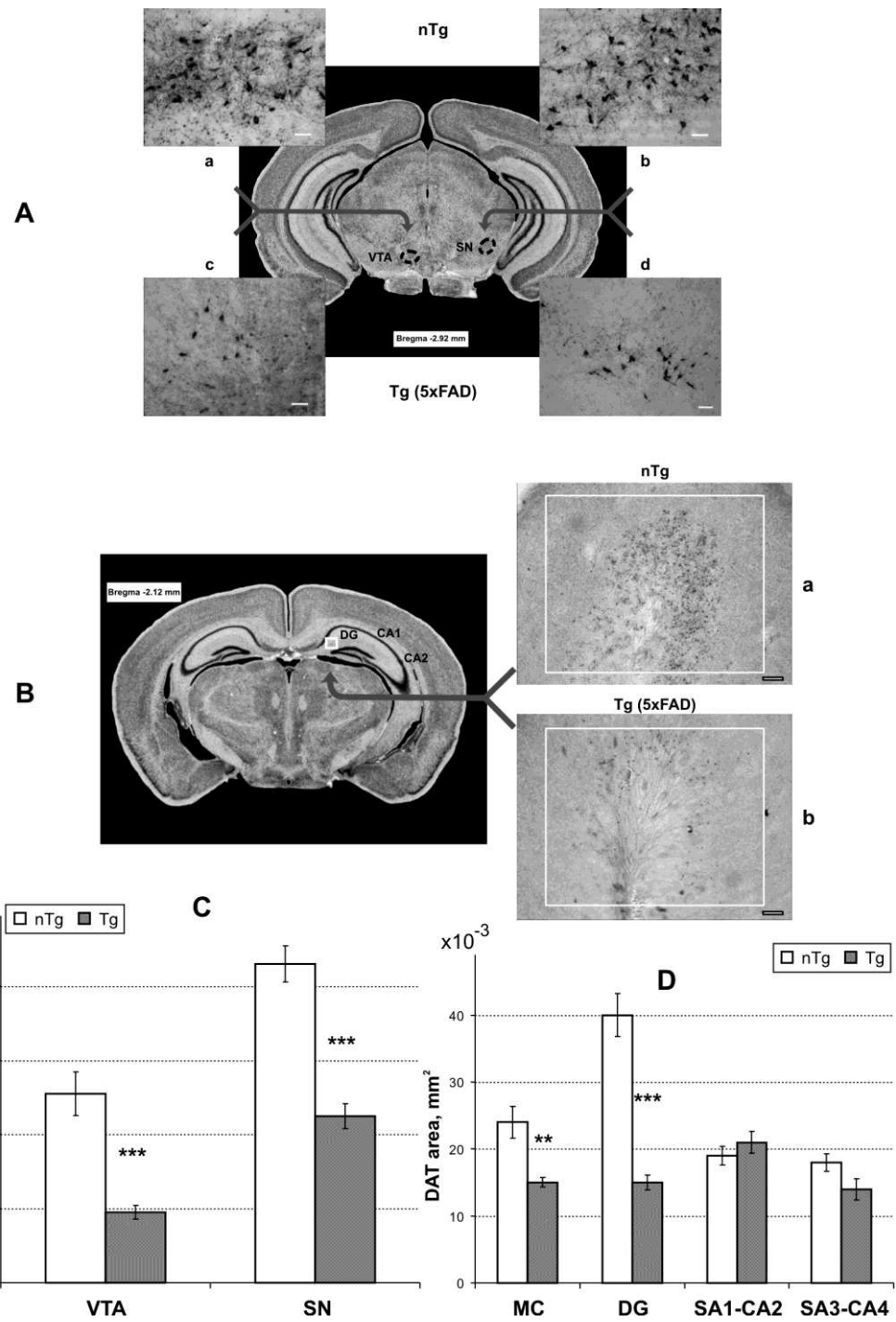


Figure 6